IMPROVE WELDED JOINTS CRYOGENIC STEEL STRUCTURE BY HARDENING TREATMENT

Melat Bormambet [1] & Remus Zăgan[2]

[1] "Ovidius" University of Constanta-Romania, Department of Welding and Harbour Equipment
Blv. Mamaia, no.124, 900527 Constanta, Romania
[2] "Ovidius" University of Constanta-Romania, Department of Economic and Engineering Technologies
Blvd. Mamaia, no.124, 900527 Constanta, Romania

Corresponding author: Remus Zăgan, remuszagan@univ-ovidius.ro

Abstract: Industrial steels utilization at low temperatures leads to different studies that tend to increase both the capacity and safety of equipment in this field. According to the exploitation temperature and utilization conditions, cryogenic materials can be classified as: Al, Cu, Ni, Ti, Li, Mg, etc. non-ferrous alloys; cryogenic irons; Ni steels; Cr-Ni austenitic steels. Out of the many steels specially made for low temperature utilization, the optimal steel brand is chosen after a detailed study of its utilization and mechanical properties.
Experimental studies and researches have been realised on 321 austenitic stainless steels with high mechanical properties at low temperatures and active atmosphere corrosion. This steel is recommended for the manufacturing of liquid nitrogen transport recipients. Metallographycal analysis and studies concerning hardness and low temperatures resistance properties have been made on manual-metal-arc (MMA) welded and deep hardening treated samples. In addition, a study by spectral analysis of metallographic structure was done.
Key words: cryogenic steel, deep hardening treatment, power spectral density, hardness, toughness.

1. INTRODUCTION

Industrial use of steel at low temperatures leads to different studies, which tend to increase both the capacity and security installations in this area.
The large number of steel specially designed for operation at low temperatures and the optimal choice of steel mark is through a thorough knowledge of the uses and mechanical properties they offer. Thus, in figure 1 are some recommendations for steel selection depending on operating temperature. Since the operating temperatures steels are known, the convenient use of these can be selected.
For liquid nitrogen storage containers (-196°C) austenitic stainless steel is recommended. Taking into account this recommendation, austenitic stainless steel 321 was chosen and its chemical composition is presented in table 1.
Predetermination steel structure studied method was ″Function Fit″ (Welding Reasearch Council, WRC diagram representation – figure 2). The diagram can be concluded that the steel structure consists of austenite and ≈9% δ ferrite. In the case of alloy steels, ferrite reduces the risk of hot cracking.

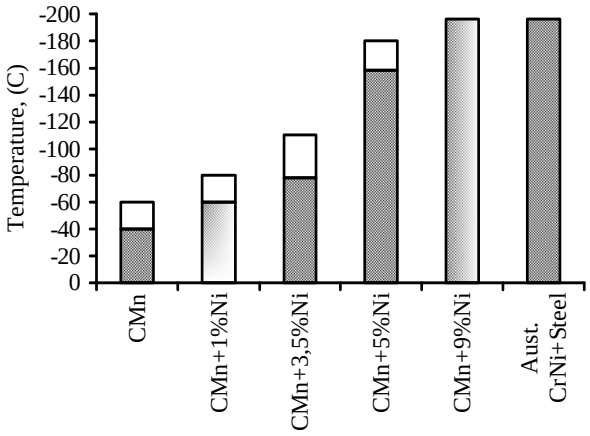

Fig. 1. Operating temperatures for different steel grades

Table 1. Chemical composition (%) steel 321

C	Si	Mn	Cr	Ni	Mo	Cu	Ti	Nb	Al	W	V	Co
0,034	0,69	1,70	18,55	9,41	0,28	0,35	0,0018	0,049	0,068	0,085	0,061	0,24

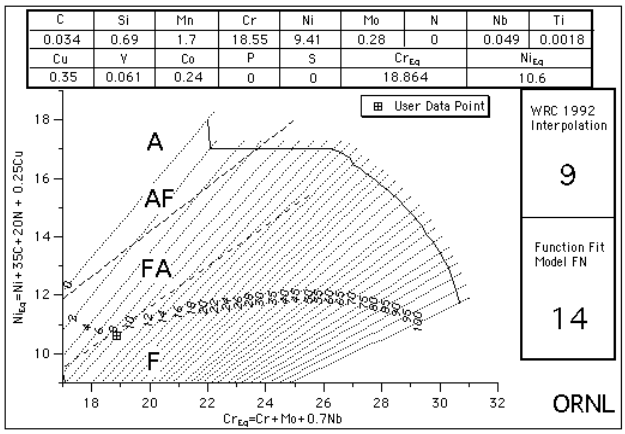

Fig. 2. WRC diagram for determining the structure and δ ferrite content of 321 steel

2. WELDING PROCEDURES AND APPLIED HEAT TREATMENT

For the experimental study was performed a sample with thickness of 12 mm welded with manual metal arc procedures – MMA (figure 3) and was subjected after welding to deep hardening treatment.
For welding was used electrode E347-15 (AWS A5.4-92), which is austenitic steel, basic coated and ensures high-joints with high quality and tenacity at temperatures up to -196°C. For welding was used welding procedure presented in table 2.

Table 2. Manual metal arc welding procedures

Sample thickness (mm)	Row	d_e, (mm)	I_s, (A)	U_a, (V)	v_s, (cm/s)	E_l, (J/cm)
12	1	3,25	100	24	0,179	10000
	2-3	4	132	27	0,281	10000

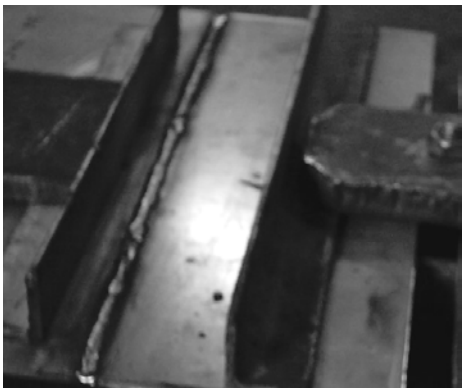

Fig. 3. Manual metal arc welding sample

To prevent overheating the base metal and to provide good protection from the atmosphere recommended welding performance by submitting rows filiform, without oscillation electrode. Row width must not exceed 1,5 times the diameter of the electrode.
The rows shall be uniform so that each not remains grooves in which to collect slag. Overlapping rows will be up to 50%.
The ratio of the intensity of welding current and electrode diameter is, usually, 30-35 A/mm. For different welding position such as horizontal position, it is not recommended the use of electrodes with a diameter less than 4 mm because it forms a larger amount of liquid metal that tends to drain, (Bormambet M., Zamfirescu G., (2004).
Deep hardening treatment applies to some stainless steels (austenitic, ferritic) whose rapid cooling does not determine occurence of martensite. In the case of austenitic steels alloyed with Mn-Ni or Cr-Ni (18-8) deep hardening treatment aims to restore the structure. If during thermal processing Cr-Ni austenitic stainless steel structure has large amount limit grain carbide precipitates, then deep hardening treatment reduces dispersion and increases there and restore the intercrystalline corrosion resistance. Putting the solution of Cr carbides is obtained by applying a heating at 1000-1100°C, calculated for the duration of maintaining uniformity and structural homogeneity and then cooling at high speed (usually in water). In this way is obtained at room temperature metastable austenite with a high degree of alloying, (Giacomelli I., et al, 2004).
Deep hardening treatment regime: heating temperature=1100°C, maintenance time=30 minute, cooling water.

3. WAVELET TRANSFORM METHODOLOGY USED TO SIGNAL PROCESSING ANALYSIS

Ultrasonic methodologies are the most practically feasible non-distrutive testing (NDT) applications in the area of material characterization. The two major parameters measured with ultrasonic technique are the attenuation and the velocity of the waves. Attenuation is determined by the energy losses in compressions and decompressions in ultrasonic waves, which include absorption and scattering contributions. After ultrasound traveled through the sample the transducer received the ultrasonic response in the time domain. A spectrum analyzer converted the ultrasonic pulse from the time domain to the frequency domain via Fourier transforms.
The technique performs two consecutive fast Fourier transforms (FFT) on the ultrasonic response signal to find the fundamental resonant frequencies. Amplitude and frequency changes in the fundamental resonant frequencies were tested from the ultrasonic responses of the samples. The power spectrum shows the energy distribution in the frequency domain and highlights the main frequency in the signal.
In the analysis of transient non-stationary ultrasonic signals, it is important to determine the time-frequency evolution of the signal, with as little distortion as possible.
The Wavelet Transform (WT) is a method of processing transient non-stationary signals simultaneously in the time domain and in the frequency domain. The WT uses scaling in the time domain to scale a single function in frequency. This function, commonly referred to as the mother wavelet, is used to extract details and information on time and frequency domains from the transient signal under analysis. This approach results in a more natural description of the signal, since the size of the window in the time domain is now a function of scaling.
The Fourier transform *F(t)* in the frequency domain is computed from *f*(t) in the time domain by the direct integration of the relation, (Petculescu P., Zăgan R., Bormambet M., 2007):

$$F(f) = \int_{-\infty}^{+\infty} f(t) e^{-j2\pi ft} dt \qquad (1)$$

The power spectrum function *G(f)* is linked with *F(t)* by the following relation:

$$G(f)=\frac{2}{T}\left|F(t)\right|^2 \tag{2}$$

The power spectrum shows the energy distribution in the frequency domain and highlights the main frequency in the signal, (Gammell M., 1981, Aurelian Vlase, et al, 2010).

The WT of a function *f(x)* corresponds to the decomposition of *f(x)* on the family of wavelets, $\left(\psi_{a,b}(x)\right)_{a\in\Re+,b\in\Re}$ generated from one single function *ψ(x)* (namely the mother wavelet) by dilatations and compressions:

$$\left(W_\psi f\right)(a,b)=\int_{-\infty}^{+\infty} f(x)\psi_{a,b}(x)dx \tag{3}$$

$$\psi_{a,b}(x)=a^{-\frac{1}{2}}\psi\left(\frac{x-b}{a}\right) \tag{4}$$

Of particular interest is the discretization on a dyadic grid ($a=2^j$, $b=2^jk$ with $(j,\ k)\in Z^2$ for which it is possible to construct functions ψ such that the set $\psi_{j,k}(x)=2^{-\frac{j}{2}}\psi\left(2^j x-k\right),\ j,k\in Z$ constitutes an orthonormal basis of square integrable functions over $L^2(R)$. On this discrete grid, the wavelet decomposition of *f(x)* becomes

$$f(x)=\sum_{j,k=-\infty}^{\infty} c_{j,k}\psi_{j,k}(x) \tag{5}$$

where the wavelet coefficients c_{ijk} are the inner products of the signal with the wavelet basis functions

$$c_{j,k}=\left\langle f,\psi_{j,k}\right\rangle \tag{6}$$

The parameters *b* and *a* are the time and frequency, respectively, so the relation (12) can be written by replacing both parameters with the time parameter *t* and frequency parameter *f*.

We must specify that the mother wavelet satisfies the admissibility condition:

$$\sum_{n=-\infty}^{\infty}\left|c_n\right|^2<\infty \tag{7}$$

The signal specific analyzing wavelet is applied to *ψ(f,t,x)*, (Petculescu R., et al, 2001, Ză gan R., et al, 2006, Dumitru Nedelcu et al, 2010).

We know that an ultrasonic transducer is sensitive to the local pressure field, and therefore generates a signal proportional to the local displacement, i.e. the square root of the potential energy. Also the magnitude of the complex analytic Wavelet Transform output thus describes the envelope of the ultrasonic signal. Furthermore, the square of this quantity is equal to the true rate of arrival of the sound energy traveling through the material.

The WT uses scaling in the time domain to scale a single function in frequency. This function, commonly referred to as mother wavelet (in our case we use the Morlet wavelet function), is used to extract details and information on time and frequency domains from transient signal under analysis. This approach results in a more natural description of the signal, since the size of the window in the time domain is now a function of the scaling.

The wavelet transform as a signal decomposition can't be directly compared to any time-frequency representation. However there is a relationship between a scale parameter and frequency, which is shown below using an example of the Morlet analyzing wavelet. The Morlet wavelet function (see figure 4) is defined as:

$$\psi(t)=e^{\frac{-|t|^2}{2}}e^{j\omega_0 t} \tag{8}$$

When dilated it can be represented in the wavelet frequency domain as

$$\Psi_a(\omega)=e^{\left[-(a\omega-\omega_0)^2\right]} \tag{9}$$

This function reaches the maximum value when $a\omega=\omega_0$ ($\omega_0=1.75\pi$). Thus the value of the dilation "*a*" at which the wavelet filter is focused on the wavelet frequency ν can be determined from

$$a_\nu=\frac{\omega_0}{2\pi\nu} \tag{10}$$

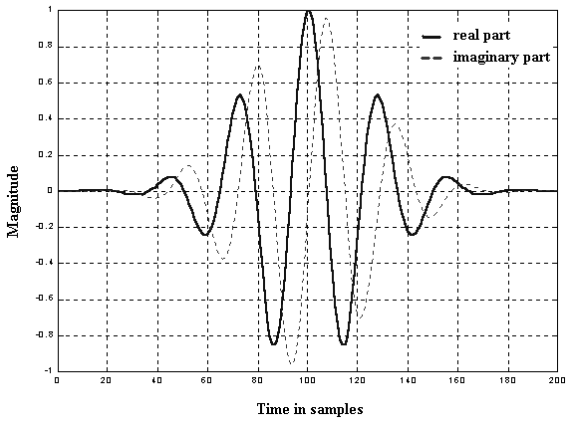

Fig. 4. Real and imaginary part of the Morlet wavelet function

The value of the frequency ν can be expressed in terms of the sampling frequency ν_ψ of the analyzing wavelet function. Since the analyzing wavelet function and the signal do not need to be sampled with the same rate, the relationship between the scale parameter "a_ν" and the signal frequency ν_w at which the analyzing wavelet function is focused can be given as

$$a_\nu=\frac{1}{\nu_w}\cdot\frac{\nu_s}{\nu_\psi}\cdot\frac{\omega_0}{2\pi} \tag{11}$$

where ν_w is the signal frequency at which the wavelet filter is focused and ν_s is the sampling frequency of the signal.

The wavelet transform means that the function *f(t)* is characterized by its decomposition of a wavelet family with a series of different frequency

bandwidths. This can be explained by working out the bandwidth of the wavelet family. The Fourier transform of the wavelet family $\sqrt{a}\psi(at)$ is

$$\Psi_a(\omega) = \frac{1}{\sqrt{a}}\Psi\left(\frac{\omega}{a}\right) \qquad (12)$$

Let consider ω_0 be the centre of the passband of $\Psi(\omega)$. Then

$$\omega_0 = \frac{\int_0^\infty \omega|\Psi(\omega)|^2 d\omega}{\int_0^\infty |\Psi(\omega)|^2 d\omega} \qquad (13)$$

For the wavelet family, the centre frequency of the passband is

$$a\omega_0 = \frac{\int_0^\infty \omega|\Psi_a(\omega)|^2 d\omega}{\int_0^\infty |\Psi_a(\omega)|^2 d\omega} \qquad (14)$$

The root mean square bandwidth of the wavelet around ω_0 is given by σ_ω, where

$$\sigma_\omega^2 = \int_0^\infty (\omega-\omega_0)^2|\Psi(\omega)|^2 d\omega \qquad (15)$$

With $\Psi(\omega)$ replaced by $\Psi_a(\omega)$ and ω_0 by $a\omega_0$ in the equation (12), the root mean square bandwidth is seen to be $a\sigma_\omega$. That is, the bandwidth of the wavelet is proportional to the scaling factor "*a*". Thus the wavelet transform produces a series of frequency channels with increasing bandwidth as the scale "*a*" changes. As the scaling factor increases, both the centre frequency and the width of the frequency band increase.

The recover of the original signal from its wavelet transform through the synthesis formula, can be given by

$$f(t) = \frac{1}{C_\psi}\int_{-\infty}^{+\infty}\int_{-\infty}^{+\infty}(W_\psi)(a,b)\frac{1}{\sqrt{a}}\overline{\psi\left(\frac{t-b}{a}\right)}\frac{dadb}{a^2} \qquad (16)$$

Many other practical applications impose additional conditions on regularity and vanishing moments on wavelets.

A square representation of the signal in the time-frequency domain is given by an energetic representation.

This representation can be interpreted as an indicator of the manner the signal energy is distributed both in time and also in frequency. The availability of the interpretation of this representation as a density of energy is also given by the way in which this representation satisfies other specific properties. Among them, there is one which requires that the integration in the time domain should represent the power spectral density (PSD) and in the frequency domain should have the meaning of a momentary power of the signal.

The power spectrum function *G(t)* is linked with *F(t)* by the following relation:

$$G(f) = \frac{2}{T}|F(t)|^2 \qquad (17)$$

The power spectrum density shows the energy distribution in the frequency domain and highlights the main frequency in the signal.

Applying FFT and WT from the frequency domain to 321 steel samples we determined typical power spectrum density (see in figure 5).

4. METALLOGRAPHIC STRUCTURE

Metallographic structure of the sample was determined by spectral analysis and metallographic analysis, (Kumar A., et al., 1999, Kumar A., et al., 2000, Marshal P., 1984, Petculescu P., et al., 2007).

Frequency spectral analysis of the sample of 321 steel welded by the MMA procedures and which was treated by deep hardening treatment highlights the following results.

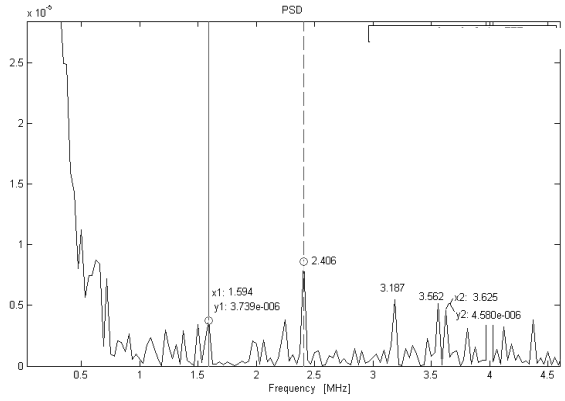

Fig. 5. Power Spectral Density (base material)

Power Spectral Density of figure 5 points to more important frequencies, with significant maximum, such as 1.594 MHz, 2.406 MHZ, 3.187 MHz, 3.562 MHz and 3.625 MHz.

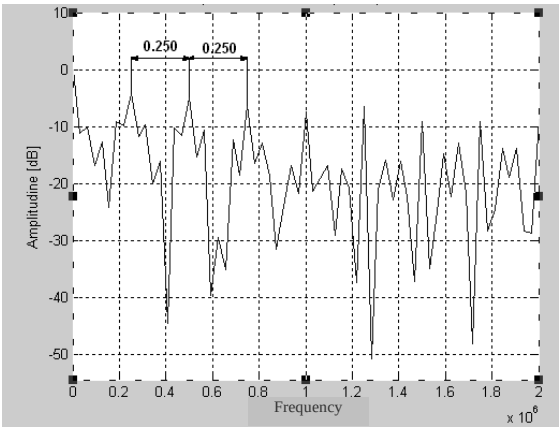

Fig. 6. Resonance spectrum (base material)

Resonance spectrum of basic material reveal the existence of f_0 = 250 KHz.

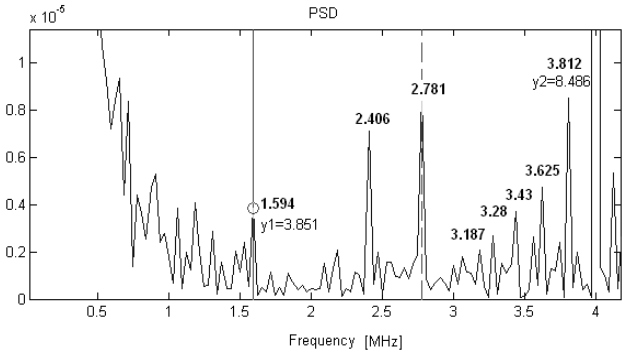

Fig. 7. Power Spectral Density (welding)

Figure 7 emphasizes the existence of several important frequencies, with significant maximum, that 1.594 MHz, 2.406 MHZ, 2.781 MHz, 3.187 MHz, 3.28 MHz, 3.43 MHz, 3.625 MHz and 3.812 MHz.

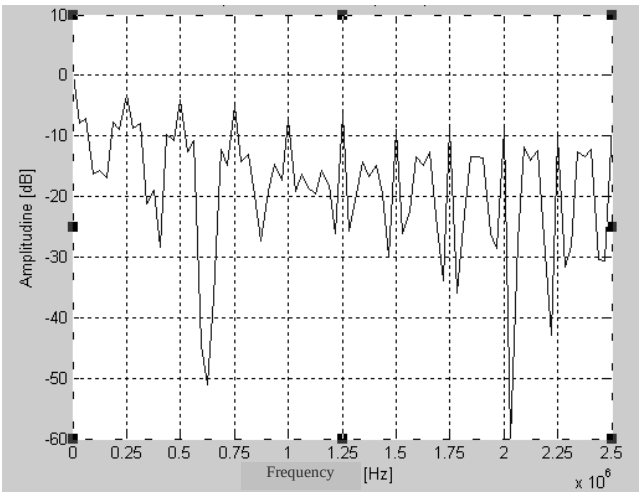

Fig. 8. Resonance spectrum (welding)

Resonance spectrum of welding material reveal the existence of f_o = 250 KHz.

Figure 9 shows the macro and microstructure of the sample.

Microstructure research has been carried out by electronic microscopy at a magnification of 200:1.

In order to highlight the microstructure sample was prepared as follows:

- preliminary polishing - was achieved with metallographic papers increasing fine abrasive particles: 100, 180, 280, 400, 500, 700, 800, 1000;
- final polishing - mechanical polishing was performed Al_2O_3 suspension with distilled water the sprayed surface periodically surface polishing cloth mounted on a rotating disc (maximum speed 400-600 revolution/minute);
- reagent application (aqua regia) - consisting of concentrated nitric acid (30 ml), concentrated hydrochloric acid (40 ml) and distilled water (40 ml). Time of attack is of a few minutes.

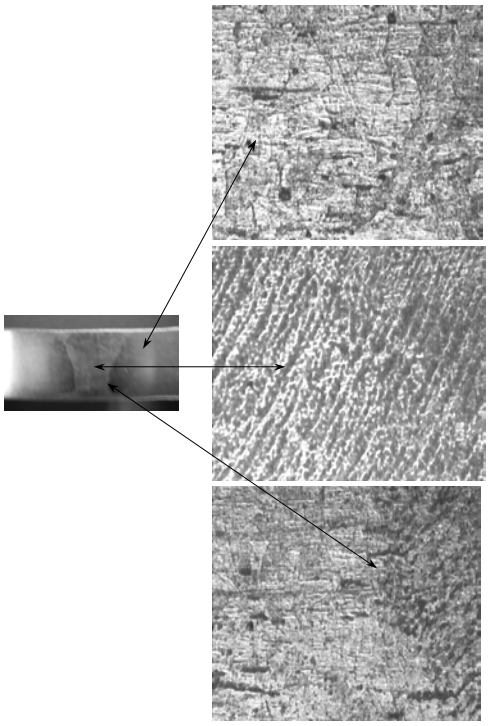

Fig. 9. Macro and microstructure of sample. Attack: aqua regia. 200:1

5. HARDNESS MEASUREMENT

The hardness was measured in the base metal (BM), heat affected zone (HAZ) and weld (W) by Vickers method through with 29.42 daN load (30 kgf) – table 3. Variation of hardness along the seam is shown in figure 10.

Table 3. Vickers hardness HV30

Row	Zone	Left		Right	
I	W	0	205	-	-
		1	192	1	201
	HAZ	2	198	2	197
	BM	3	182	3	184
II	W	0	205	-	-
		1	200	1	203
	HAZ	2	195	2	194
	BM	3	185	3	184

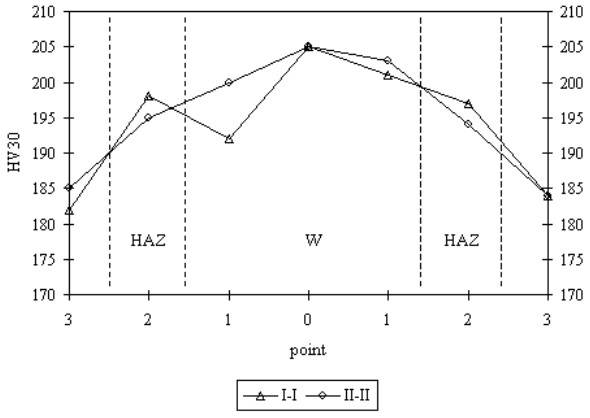

Fig. 10. HV30 hardness variation of welded seam

6. TOUGHNESS DETERMINATION

Tests for determining the characteristics of dynamic toughness were performed on samples with V notch in weld. To determine the toughness at a temperature of –196°C was used as the medium of liquid nitrogen cooling. Table 4 presents average values of kV breaking energy and KCV resilience if the sample studied.

Table 4. kV breaking energy and KCV resilience Charpy V specimens obtained

Testing temperature (°C)	Average values of breaking energy (J)	KCV resilience (J/cm^2)
+20	55,50	69,37
-196	30,00	37,50

7. CONCLUSIONS

Metallographic analysis of the sample reveals the following structure:
- the seam structure is cast-looking dendritic solidification and structural constituents are austenite and δ ferrite. It also notes the presence of Cr carbide precipitates;
- in the transition, the structure is affected by heating a small thickness; heating and rapid cooling led to fragmentation of the initial austenite crystals;
- the basic material structure consists of polyhedral crystals of austenite with numerous macle bands, δ ferrite and a lesser amount of carbide precipitates at grain limit.

Taking into account the peaks in the PSD diagram and making the report frequency amplitude of the smallest size and size of the largest amplitude frequency can be calculated Spectral Peak Ratio - SPR.
SPR = 3.739 / 4.580 = 0.814 (in base material)
SPR = 3.851 / 8.486 = 0.453 (in weld)
Spectrum reveals in material base the existence of following constituents: ferrite (peak frequency 1.594 MHz); austenite (peak frequency 2.406 MHz); different Cr carbide precipitates at grain limit (peak frequencies 3.187, 3.562 and 3.625 MHz).
Spectrum reveals in weld material the existence of following constituents: ferrite (peak frequency 1.594 MHz); austenite (peak frequency 2.406 MHz); more Cr carbide precipitates at grain limit (peak frequencies 3.187, 3.28, 3.43, 3.625 and 3.812 MHz).
The spectral analysis performed following conclusions can be mentioned:
-existence of the same frequency peaks in both the basic material, and the weld, highlights the compatibility of the two materials, so the heat treatment did not change the material structure;
-for SPR= 0.814, in base material grain size is 46.6 μm, its structure is mostly austenitic, and in weld for SPR=0.453, grain size is de 42.38 μm, with a structure consisting of austenite+ferrite+Cr carbide.
In terms of hardness can be concluded that deep hardening treatment application did not lead to a hardening of seam, values remained within acceptable limits.
In the case of 321 steel welding with manual metal arc procedures can appreciate a good tenacity of sample subjected to heat treatment. Welding material toughness does not decrease below which plant operation would be dangerous in cryogenic field.

8. REFERENCES

1. Bormambet M., Zamfirescu G., (2004). *Experimental Researches Concerning Behaviour of Welding Cryogenic Steels*, Proceedings of ″Sudura 2004″ International Conference, pp.109-116.
2. Gammell M., (1981). *Analogue implementation of analytic signal processing for pulse-echo systems*, Ultrasonics, pp. 279-283.
3. Giacomelli I., Bormambet M., Zamfirescu G. (2004). *Materiale şi tratamente termice pentru produse sudate*, Editura Ovidius University Press, ISBN 973-614-192-6, Constanţa.
4. Kumar A., Jayakumar T., Palanichamy P. & Baldev R. (1999). *Influence of grain size on ultrasonic spectral parameters in AISI type 316 stainless steel*, Scripta Materialia, Vol. 40, No. 3, pp. 333.
5. Kumar A., Jayakumar T., Baldev R. (2000). *Ultrasonic spectral analysis for microstructural characterization of austenitic and ferritic steels*, Philosophical Magazine A, Vol. 80, No. 11, pp. 2469-2487.
6. Marshal P. (1984). *Austenitic stainless steels microstructure and properties*, Elsevier, London
7. Petculescu R., Ciocan D., Ciobanu, C., (2001). *Automated system and automated method by ultrasonic investigation*, Patent No. 118612B, RO.
8. Petculescu P., Zăgan R., Bormambet M. (2007). *The influence of thermal treatments on acoustical-spectral parameters*, Journal of Optoelectronics and Advanced Materials, Vol. 9, No. 12, pp. 3847-3851.
9. Zăgan R., Petculescu P., Peride N. (2006). *Analyse of frequency spectrum in austenitic steel sample*, Proceedings of European Conference of Physics, Dresda.
10. Dumitru Nedelcu, Olivera Milosevic, Romeu Chelariu & Costel Roman, (2010). *Some experimental aspects concerninq the stratified composite materials with metallic matrix*, Int. J. of Modern Manufacturing Technologies, II(2), pp. 65-71.
11. Aurelian Vlase, Bogdan Vlase & Ruxandra Balan, (2010). *New functions of the surface roughness when cutting the stainless steel 10NiCr180 and OLC45*, Int. J. of Modern Manufacturing Technologies, II(1), pp. 99-104.

Received: September 1, 2011 / Accepted: November 30, 2011 / Paper available online: December 10, 2011
© International Journal of Modern Manufacturing Technologies